PCCP

Accepted Manuscript

ROYAL SOCIETY OF CHEMISTRY

www.rsc.org/pccp

A novel Pd_3O_9@α-Al_2O_3 catalyst under hydroxylated effect: high activity in CO oxidation reaction

Qiaohong Li, Yongqin Wei, Rongjian Sa, Zuju Ma and Kechen Wu*

State Key Laboratory of Structural Chemistry, Fujian Institute of Research on the Structure of Matter, Chinese Academy of Sciences, Fuzhou 350002, PR China

ABSTRACT

Considering the importance of palladium-based and doped metal-oxide catalysts in CO oxidation, we design a new Pd_3O_9@α-Al_2O_3 catalyst and simulate its efficiency under a hydroxylated effect. The structure, electronic structure and oxidation activity of hydroxylated Pd_3O_9@α-Al_2O_3(0001) surface are investigated by density functional theory. Under the O-rich growth condition, Pd preferentially replaces Al. The lowest formation energy of the Pd-doped α-Al_2O_3(0001) surface is 0.21 eV in the condition under which the coverage of the Pd-doped α-Al_2O_3 is 0.75 on a pre-hydroxylated surface and the water coverage is 0.25, which leads to formation of a Pd_3O_9 cluster embedded in the Al_2O_3(0001) surface. The reaction mechanisms of CO oxidization have been elucidated first by CO adsorption and migration, second by O_v formation with the first CO_2 release, then by the first foreign O_2 filling and CO co-adsorption, and finally by the second CO_2 desorption and restoration of the hydroxylated Pd_3O_9@α-Al_2O_3(0001) surface. The rate determination step is the formation of the first CO_2 in the whole catalytic cycle. The results also indicate that the energy barrier for CO oxidization is obviously reduced compared to the undoped surface, which

* Corresponding author. Fax: +86 591 83792932.
E-mail address: wkc@fjirsm.ac.cn (K. Wu).

implies that the introduction of Pd can efficiently improve the oxidation reactivity of the α-Al_2O_3(0001) surface. Compared to the synthesized Ir_1/FeO_x (1.41 eV) and Pt_1/FeO_x (0.79 eV) catalyst, the reaction activation barrier of CO oxidation is lowered by 0.65 eV and 0.03 eV, respectively. Therefore, the Pd_3O_9@α-Al_2O_3 catalyst shows superior catalytic activity in CO oxidation. The present results enrich the understanding of the catalytic oxidation of CO by palladium-based catalysts and provide a clue for fabricating palladium-based catalysts with low cost and high activity.

Keywords: carbon oxide, hydroxylation, palladium, α-Al_2O_3, DFT

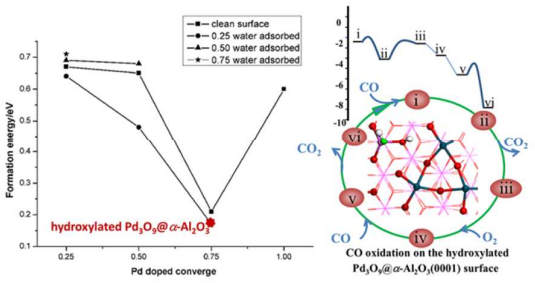

A new $Pd_3O_9@\alpha$-Al_2O_3 catalyst has been designed and shows superior catalytic activity for CO oxidation.

1. Introduction

The concept of catalytic active sites has widely gained ground in homogeneous and heterogeneous catalysts[1-4]. Supported metal nanostructures, the size of which is a key factor in determining the performance of such catalysts, are the most widely used type of heterogeneous catalyst in industrial processes[2, 5-9]. The low-coordinated metal atoms in those catalysts often act as catalytically active sites. Therefore, in heterogeneous catalysis, one of the significant targets is to explore the relationship between the catalytic behaviour and electronic structure of the active sites to assist in optimizing and designing a new catalyst with high activity and selectivity.

The surface free energy of metal species, as is known to all, increases rapidly with reduction in the size of metal particles, which will facilitate the activation of these metal species and thus generate more dangling bonds and empty *d* atomic orbitals of metal species on the surface. Therefore, it is the ultimate goal and challenge of heterogeneous catalysis to downsize the particles or clusters in the supported noble-metal catalysts.

Substitution cation doping is not the only possibility. There is evidence that the presence of a large collection of doped oxides. Noble metals Pt, Pd Au, and Rh supported on conventional materials such as alumina, zirconia, ceria, iron oxide and titania have been studied[2, 10-17]. Zhang's group[2, 16, 18, 19] fabricated a series of single-atom catalysts (SAC) Pt_1/FeO_x and Ir_1/FeO_x, which exhibit high activities and significant stabilities for CO oxidation. The rate-determining step in the catalytic cycle of CO oxidation has been reported to be the formation of the second CO_2.

Peterson et al[20] reported low-temperature carbon monoxide oxidation catalyzed by re-generable atomically dispersed palladium on alumina, and aberration-corrected scanning transmission electron microcopy (STEM) and X-ray adsorption spectroscopy confirmed that isolated palladium atoms can be catalytically active on industrially relevant γ–alumina supports. Narula[15] and his co-workers studied Pt atoms on a θ-Al_2O_3 (010) surface and found that CO oxidation on a single Pt atom cannot occur via a conventional Langmuir-Hinshelwood scheme (L-H scheme), which requires at least one Pt-Pt bond. There are only a few experimental examples of supported single-atom catalysts, whereas a host of theoretical investigations have been reported[10, 12, 13, 17, 19, 21]. Li[12] investigated formaldehyde oxidation on the Pt/TiO_2(101) surface to map out the reaction network. A single Pd atom embedded in CeO_2(111) for a reaction between NO and CO was studied by Li[17], who described in detail the formation of a Pd_1-O_v pair and the synergetic effect between a Pd 4*d* electron and the reducibility of CeO_2 by electronic structure analysis. Recently, Liu[22] investigated the electronic structure and reactivity of Pt atoms stabilized by vacancy defects on hexagonal boron nitride (h-BN) by first principles-based calculations, and the barriers for CO oxidation were 0.38, 0.1 and 0.04 eV, suggesting the superiority of PtBV as a catalyst for low-temperature CO oxidation. However, so far, little has been reported on the Pd-doped hydroxylated α-Al_2O_3(0001) surface. Considering the importance of palladium-based and doped metal-oxide catalysts in CO oxidation, the study herein focuses on simulating novel catalysts with noble metals supported on conventional materials, which not only reduces the amount of high-priced noble ones

in the catalyst but also improves the catalytic activity through an oxide made by substituting a small fraction of cations in a "host oxide" with a different cation. Over the past decade, the value of modelling doped oxide (metal/metal oxide) interactions has been illustrated by many studies concerning the modelling of metal atoms and nanoparticles on metal oxides[20, 23-25]. Owing to their numerous applications, Pd/Al_2O_3 and Pt/Al_2O_3 are the most commonly studied systems[24-28]. However, Pd doped on α-Al_2O_3(0001) with a Pd_3O_9 cluster has been rarely considered. Several studies have observed the adsorption of water molecules onto the α-Al_2O_3(0001) surface because it has been found that a clean, H-free and Al-terminated (0001) Al_2O_3 surface readily reacts with water to form surface hydroxyls. In this paper, we present a detailed comparison of the formation energy in the different doped coverage and the water adsorbed coverage with an in-depth analysis through structures, relative stabilities, and electronic structures of a clean and hydroxylated Pd@α-Al_2O_3(0001) surface (denoted as hy- Pd@α-Al_2O_3).

CO oxidation is of particular interest and has been extensively investigated over the past 40 years, and a number of noble metals (e.g., Pt, Au, Ir, Pd, Cu)[2, 21, 29-37] and metal oxides[38, 39] have been identified as active catalysts for CO oxidation. Nano Pd-based heterogeneous catalysts have been demonstrated to be active for CO oxidation[7, 20, 40, 41]. Therefore, it would be of great interest to investigate the detailed reaction mechanism of CO oxidation on a Pd@α-Al_2O_3 catalyst. To elucidate the nature of the binding of Pd_3O_9 clusters to α-Al_2O_3 support and the mechanism of CO oxidation on this Pd@α-Al_2O_3 catalyst with hydroxylation, we have performed

extensive theoretical investigations using density functional theory (DFT) on the possible catalytic reaction pathways of CO oxidation on the hydroxylated Pd_3O_9@α-Al_2O_3 (defined as hy-Pd_3O_9 @α-Al_2O_3) and the electronic structural properties of the reactants, transition states, and intermediate products. Mulliken charge analyses and density of states (DOS) have also been studied to evaluate the performance of Pd_3O_9@α-Al_2O_3 catalyst for CO oxidation. The results will enrich the understanding of the catalytic oxidation of CO by palladium-based catalysts and provide a basis for fabricating palladium-based catalysts at low cost and with high activity.

2. Computational detail

Following previous work[42, 43], the most stable (0001) surface plane for a clean α-Al_2O_3(0001) surface is formed by nonpolar termination with an Al-OOO-Al repeat pattern. Our surface is described by a 15-layer thick slab (five Al-OOO-Al repeated patterns) with a p(2×2) configuration (Fig. 1). Without the adsorbate, the vacuum

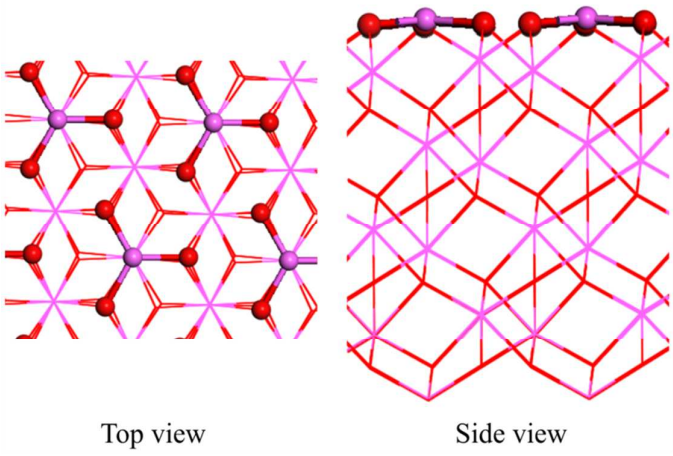

Fig. 1. Top view of the optimized stable geometry of the α-Al_2O_3(0001) surface.

between the slabs is set to span a range of 13 Å. All atoms in the five bottom layers are fixed to the bulk positions. The adsorbate is set on one side of the slab.

All calculations are performed according to the DFT approach using the Dmol software package[44, 45], which can simulate periodic systems. The generalized gradient approximation (GGA) is adopted to describe the density functional using the Perdew-Wang (PW91)[46] functional for the exchange-correlation term. The reliability of the method has been confirmed by previous reports regarding the adsorption on the Al_2O_3 surface[20, 42]. The wave functions are expanded in terms of numerical basis sets. The double-numeric quality basis set with polarisation functions (DNP[44, 47, 48]) is adopted, which is comparable to 6-31G**[49-51]. The numerical basis sets can minimise the basis set superposition error[52]. A Fermi smearing of 0.005 hartree is utilized, and a Monkhorst-Pack *k*-point grid of size of 3×3×1 is used for structural relaxation and TSs location. The tolerances of the energy, gradient and displacement convergence are 1×10^{-5} hartree, 2×10^{-3} hartree/Å, and 5×10^{-3} Å, respectively. The transition states (TS) are located using the complete linear synchronous transit/quadratic synchronous transit (LST/QST) methods.

The adsorption energies ΔE_{ads} are defined as follows:

$$\Delta E_{ads} = E_{total} - [E_{slab} + E_{adsorbate}] \quad (1)$$

where E_{total} represents the total energy for the slabs with adsorbate. E_{slab} represents the total energy of the bare slab of the surface. $E_{adsorbate}$ represents the total energies of free adsorbate molecules.

3. Results and discussion

3.1 Structures and relative stabilities of the hydroxylated Pd@α-Al_2O_3(0001) surface.

As many previous studies have shown[42, 43], the surface is characterized by a strong inward relaxation of the topmost aluminium layer into the following oxygen layer at the same level to create an Al-O surface. Furthermore, dissociated adsorption of water is found to be stable, and the most stable hydroxylation form on the clean surface is found to be in the 1–2 dissociation configurations[43], with the OH group binding to the top of the surface Al layer and the H^+ ion of H_2O binding to the surface O atom. Our work agrees with those results. Pd replaced surface Al in our model for Pd-doped clean and hydroxylated α-Al_2O_3(0001) surface (defined as hy-α-Al_2O_3).

To compare the relative stability of the various structures, the formation energy (ΔE_{form}) is used. This is derived from the formation energy of Pd@Al_2O_3 starting from a clean or hydroxylated Al_2O_3(0001) surface and bulk Pd[53-57].

$$Al_{2m}O_{3m}(0001) + n\ Pd \rightarrow nPd@Al_{2m-n}O_{3m}(0001) + n\ Al \quad (2)$$

where m is the number of Al_2O_3 units in a surface unit cell and n is the number of Pd atoms in a surface unit cell. The formation energies ΔE_{form} are defined as follows,

$$\Delta E_{form} = \frac{1}{n}[E_{nPd@\,Al_{2m-n}O_{3m}(0001)} + n\mu_{Al} - E_{Al_{2m}O_{3m}(0001)} - n\mu_{Pd}] \quad (3)$$

Where n is the number of doped Pd atoms; $E_{nPd@Al_{2m-n}O_{3m}(0001)}$ and $E_{Al_{2m}O_{3m}(0001)}$ are the total energies of the Al_2O_3(0001) surface with and without dopant, respectively; μ_{Al} and μ_{Pd} are the chemical potentials of the aluminium and palladium atoms, respectively. In eq. 3, the formation energy is not fixed but depends on the growth

condition, including O-rich and O-poor conditions. Under the O-poor condition, μ_{Al} and μ_{Pd} are assumed to be the energy of bulk Al and Pd, respectively. Under the O-rich condition, the chemical potential of the O atom, μ_O, is obtained from the ground-state energy of the O_2 molecule—that is, $\mu_O = \frac{1}{2}\mu_{O_2}$—and the chemical potentials of Al and Pd are calculated by the thermodynamic equilibrium relation, which is defined as follows:

$$\mu_{Pd} + \mu_O = \mu_{PdO}^{bulk} \quad (4)$$

$$2\mu_{Al} + 3\mu_O = \mu_{Al_2O_3}^{bulk} \quad (5)$$

With respect to the dopant atom Pd, the chemical potential $\mu_{Pd} = \mu_{PdO}^{bulk} - \frac{1}{2}\mu_{O_2}$ from the corresponding metal oxide (namely, PdO). Moreover, the chemical potential $\mu_{Al} = \frac{1}{2}(\mu_{Al_2O_3}^{bulk} - \frac{3}{2}\mu_{O_2})$.

Table 1 and Fig. 2 list the formation energies of various Pd-doped clean and hydroxylated Al_2O_3(0001) surface under O-rich and O-poor conditions. To investigate the effect of Pd doping, the coverages of 0.25, 0.50, 0.75 and 1.00 are analyzed with respect to surface relaxation modes. According to the values of ΔE_{form}, it can be seen clearly that the Pd atom occupies preferentially at the coverage of 0.75 for both O-rich and O-poor conditions. Because the smaller values of ΔE_{form} are obtained for a Pd-doped clean and hydroxylated Al_2O_3(0001) surface under the O-rich growth condition, the introduction of Pd is preferential under O-rich conditions.

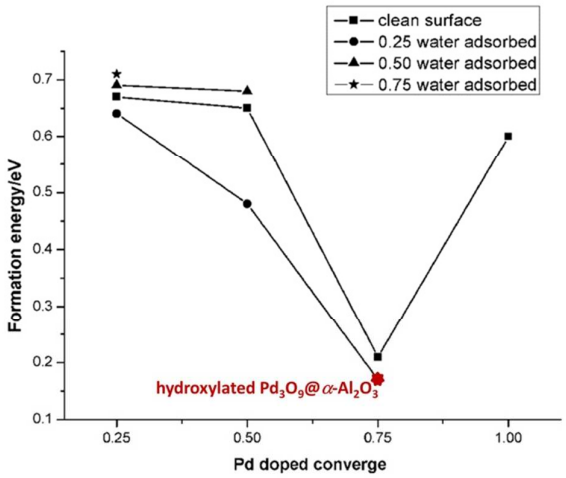

Fig. 2. The formation energy (ΔE_{form}, eV) of adsorbed H_2O onto a Pd@α-Al_2O_3(0001) surface.

Table 1. The formation energy (ΔE_{form}, eV) of adsorbed H_2O onto a Pd@α-Al_2O_3(0001) surface. hydroxylated coverage on the top surface is defined as θ_{water}, and doped coverage on the top surface is defined as D_{Pd}.

	growth condition	**D_{pd}=0.25**	**D_{pd}=0.5**	**D_{pd}=0.75**	**D_{pd}=1**
clean	O-rich	0.67	0.65	0.21	0.60
surface	O-poor	7.51	7.49	7.05	7.44
θ_{water}=0.25	O-rich	0.64	0.48	0.17	
	O-poor	7.49	7.32	7.01	
θ_{water}=0.50	O-rich	0.69	0.68		
	O-poor	7.53	7.52		
θ_{water}=0.75	O-rich	0.71			
	O-poor	7.55			

Moreover, to further investigate the effect of hydroxylation, water adsorption values of 0.25, 0.50 and 0.75 are considered. Our results indicate that the most stable hydroxylation is at θ_{water}=0.25. Therefore, we pay close attention to the structural and electronic properties of the Pd-doped coverage (D_{pd}=0.75) and hydroxylated coverage (θ_{water}=0.25) on the Al_2O_3(0001) surface, which is denoted as Pd_3O_9@α-Al_2O_3.

The results of geometry optimization for eight clean and hy-Pd@α-Al_2O_3 models

are shown in Table 2 and Fig. 3. Compared to the pure Al_2O_3(0001) surface, the substitution of Pd atoms has some influence on the surface relaxation. Owing to the Pd-doped α-Al_2O_3(0001) surface, there is the obvious enhancement of the surface relaxation in which surface reconstruction occurs. Owing to the substituting effect, the Pd atoms in the hy-Pd@α-Al_2O_3, hy-2Pd@α-Al_2O_3, and hy-3Pd@α-Al_2O_3 drive up 0.476 Å, 0.562 Å and 0.698 Å on average, respectively. Moreover, the outward movements for the surface O atoms around Pd atoms (O_{Pd}) are between 0.043 Å and 0.066 Å. However, the surface Al atoms drop slightly except for the 3Pd@α-Al_2O_3 model, and the surface O atoms near Al atoms (O_{Al}) decrease as well. Furthermore, because of the hydroxylated effect, the slight elongation of Al-O and Pd-O bond lengths is larger than those on unhydroxylated surface. Attention must be paid to the hy-3Pd@α-Al_2O_3 model, in which ΔE_{form} is the smallest and represents the outward movements for Pd atoms, and the average length of the Pd-O bond is the largest. We also found that the oxygen coordination number of Pd changes from three to four, and part of the surface O atoms (O_s) change from three coordinations (O_{3f}) to four coordinations (O_{4f}). Three Pd atoms around oxygen atoms form a Pd_3O_9 cluster, which embeds into the Al_2O_3(0001) surface. Moreover, Pd atoms rise on the surface, pyramiding with four neighbouring O atoms. Thus, the effect of Pd doping is not to be neglected, or it will result in the destruction of the geometric structures of the α-Al_2O_3 surface.

Table 2. Optimized structural parameters with respect to the clean α-Al_2O_3(0001) surface for different Pd-doped or hydroxylated α-Al_2O_3(0001) surfaces.

	hy-α-Al_2O_3	Pd@α-Al_2O_3	2Pd@α-Al_2O_3	3Pd@α-Al_2O_3	4Pd@α-Al_2O_3	[m]hy-Pd@α-Al_2O_3	hy-2Pd@α-Al_2O_3	hy-3Pd@α-Al_2O_3
Displacement (Å) along the [001] direction compared to the ideal α-Al_2O_3 (0001) surface[h]								
Pd[a]	-	0.686	0.675	0.480	0.669	0.698	0.562	0.476
O_{Pd}[b]	-	0.044	0.047	0.066	0.043	0.053	0.050	0.066
Al[c]	-0.063	-0.023	-0.043	0.043	-	-0.043	-0.388	-
O_{Al}[d]	-0.003	-0.004	-0.010	-0.019	-	-0.013	-0.032	-
Al_{OH}[e]	0.612	-	-	-	-	0.609	0.631	0.609
Bond length (Å)								
Al-O[f]	1.706	1.703	1.705	1.702	-	1.711	1.736	-
Pd-O[g]	-	1.949	1.958	2.026	1.964	1.952	1.967	2.029

[a]: surface Pd atom; [b]: surface O atom bonding with Pd; [c]: surface Al atom; [d]: surface O atom bonding with Al; [e]: surface Al atom adsorbed OH group; [f]: average bond of surface Al-O; [g]: average bond of surface Pd-O. [h]:The negative and positive values indicate that the atom moves toward the bulk and vacuum sides, respectively. [m]: hy is defined as hydroxylated.

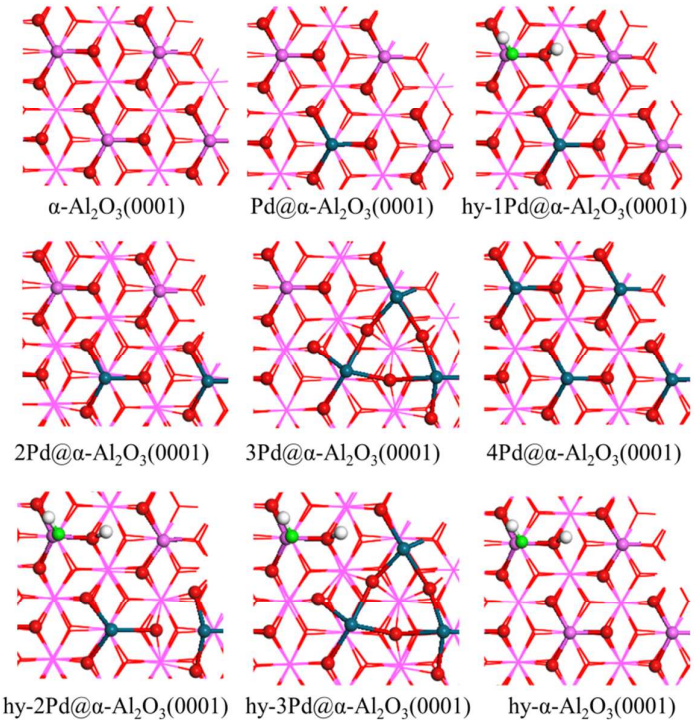

Fig. 3. Top view of the optimised stable geometry. hy is defined as hydroxylated.

3.2 Electronic structures of clean and hydroxylated Pd_3O_9@α-Al_2O_3(0001) surfaces

The total density of states (DOS) of a clean α-Al_2O_3(0001) surface, Pd-doped clean and hydroxylated Pd-doped α-Al_2O_3(0001) surface are shown in Fig. 2S (seeing surpplementary), which depicts a clear splitting at the Fermi energy and some states shifting down in energy above the Fermi energy.

At the same time, hydroxylation has a litter effect on the total DOS in general. From Fig. 4, the partial DOS of surface atoms on the Pd_3O_9@α-Al_2O_3(0001), bulk Pd and O_{3f} of clean α-Al_2O_3(0001) are demonstrated. For the substitution of Pd, we can see a clear splitting of the *p* orbital of the closest oxygen; not only O_{3f_Pd} but also O_{4f_Pd}. This splitting of the *p* orbital with the *d* orbital of the depoted Pd atom creates an antibonding state above the Fermi energy, indicating that the bonds are formed between the metal and the oxygen, as observed by Briquet for the adsorption of Pd on the (0001) surface of α-alumina[42]. A splitting of the *d* band for Pd is also observed at the Fermi level as well as the *p* band of the oxygen. Besides, compared with DOS of bulk Pd, the DOS of Pd atom are upshifted, which is accord with PtN3[58]. This kind of shift implies the activation of adsorbates would be easy activated by the transfer of the Pd-d electron from Pd_3O_9.

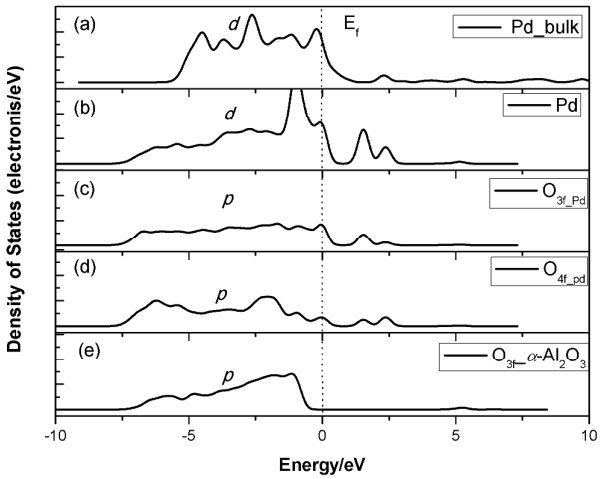

Fig. 4. Partial DOS of Pd_3O_9@α-Al_2O_3(0001) surface. The Fermi level is set at zero. O_{3f_pd} defines the three-coordination surface O atom, which is close to the Pd atom; and O_{4f} defines the four-coordination surface O atom, which is close to Pd atom.

From Fig. 5, we see the value of the Mulliken charge of clean α-Al_2O_3(0001) surface, 3Pd@α-Al_2O_3(0001) surface and hy-3Pd/α-Al_2O_3(0001). Compared to the undoped Al_2O_3, it is found that the total charge on the surface AlO_3 group is negative and accepts some electrons. With hydroxylation or without, the total charge of the Pd_3O_9 group is also negative and accepts some electrons. Furthermore, the Pd_3O_9 group, especially with the hydroxylation effect, obtains more electrons than the AlO_3 group. Next, O_{3f_Pd} and O_{4f_Pd} obtain fewer electrons from Pd atoms than O_{Al} obtains from Al atoms. The hydroxylation makes the charge of Pd atoms in the Pd_3O_9 clusters unequal.

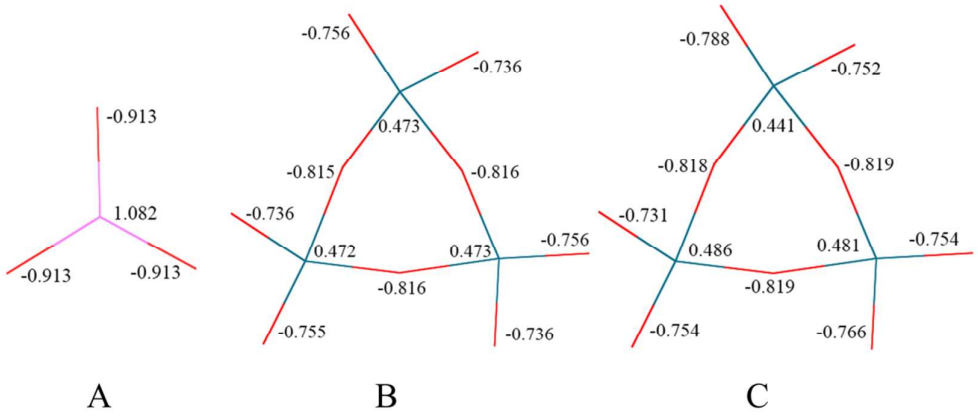

Fig. 5. The value of Mulliken charges for clean α-Al_2O_3(0001) surface (A), Pd_3O_9@α-Al_2O_3(0001) surface (B) and hy-Pd_3O_9@α-Al_2O_3(0001) (C). The pink, dark blue, and red sticks denote Al, Pd and O atoms, respectively.

With the combination of optimized structure and partial DOS and Mulliken charges, the O_{Pd} atoms are easier to remove and are also more reactive. The subsequent formation of an oxygen vacancy will benefit from a strong acid-base

interaction, and the energy to form a vacancy will be lowered by this interaction.

3.3 Catalytic CO oxidation cycle on a hydroxylated Pd_3O_9@α-Al_2O_3(0001) surface

The reaction mechanism for CO oxidation on a hydroxylated Pd_3O_9@α-Al_2O_3(0001) surface has been studied. The initial step of the reaction involves the formation of complexes in which the CO binds to the hydroxylated Pd_3O_9@α-Al_2O_3(0001) surface. After testing different possible adsorption configurations, we found eight that were stable.

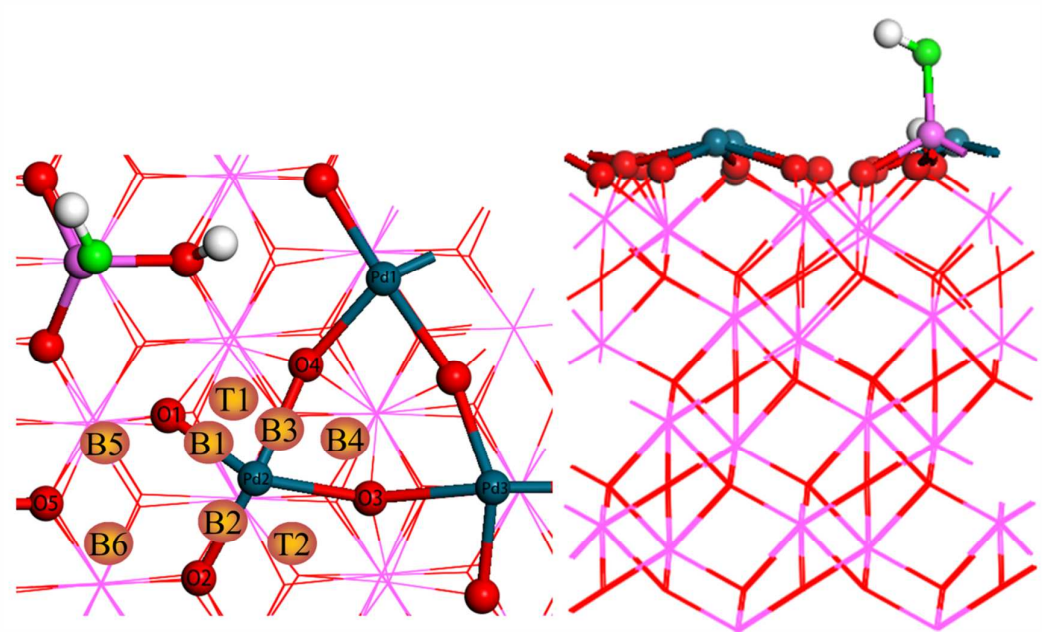

Fig. 6. Top and side views of the optimised stable geometry for Hy-Pd_3O_9@α-Al_2O_3(0001) surface. The dark blue, pink, red, green and white balls denote Pd, Al, O, O in OH and H atoms, respectively. The same colour scheme is applied in **Figs. 7–11**.

Table 3 and Figs. 6 and 7 depict CO binding to the surface in eight modes with the carbon atom approaching the surface [*i.e.*, *top* modes (T1 and T2), Pd-O *bridge* modes (B1, B2 and B3), and intermediate carbonate-like CO_3 modes (B4, B5 and

B6)]. The CO molecule preferably coordinates through its C atom. The most favourable adsorption site is the B2 site, which has an adsorption energy of -2.13 eV. The CO molecule preferably coordinates to the surface with bridge codes. Then, the CO migrates (from B2 to B6), resulting in the formation of the intermediate (carbonate-like, CO_3) with an adsorption energy of -3.04 eV (see Fig. 8). In this process, the CO molecule overcomes an activation barrier of 0.59 eV while releasing 0.91 eV of heat. In addition, from the structure analysis (see Table 3), we can see that the C-O distance is slightly elongated, especially in the *bridge* modes.

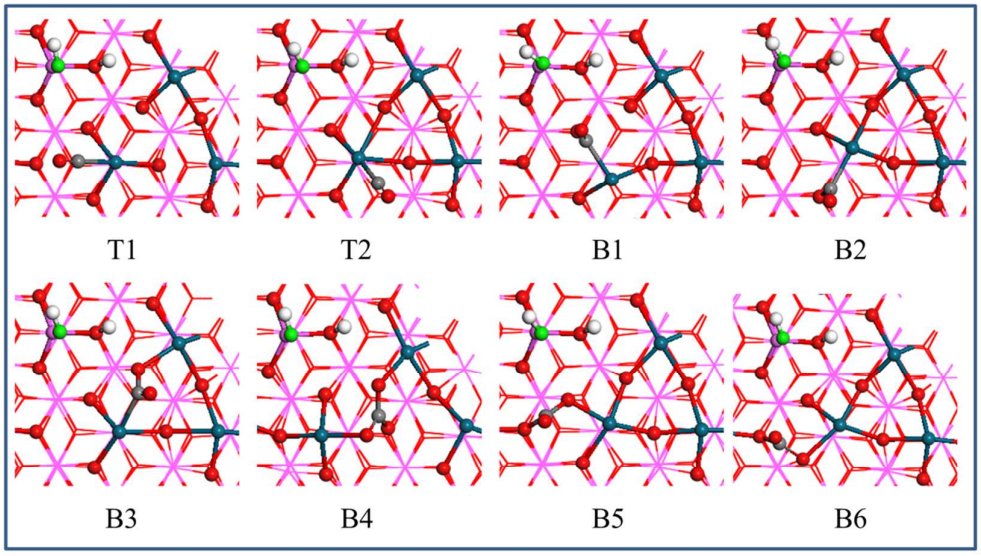

Fig. 7. Top view of the optimized stable geometry of single CO adsorption on hy-Pd_3O_9@α-Al_2O_3(0001) surface.

Table 3. The adsorption energy (in eV) and bond length (in Å) of eight modes in which the CO binds to the hy-Pd_3O_9@α-Al_2O_3(0001) surface.

	T1	T2	B1	B2	B3	intermediate		
						B4	B5	B6
E_{ads}	-0.90	-0.91	-1.74	-2.13	-1.61	-2.48	-2.68	-3.04
C-O	1.148	1.148	1.204	1.210	1.209	1.291	1.205	1.201
Pd-C	1.930	1.932	1.986	1.986	1.989	-	-	-

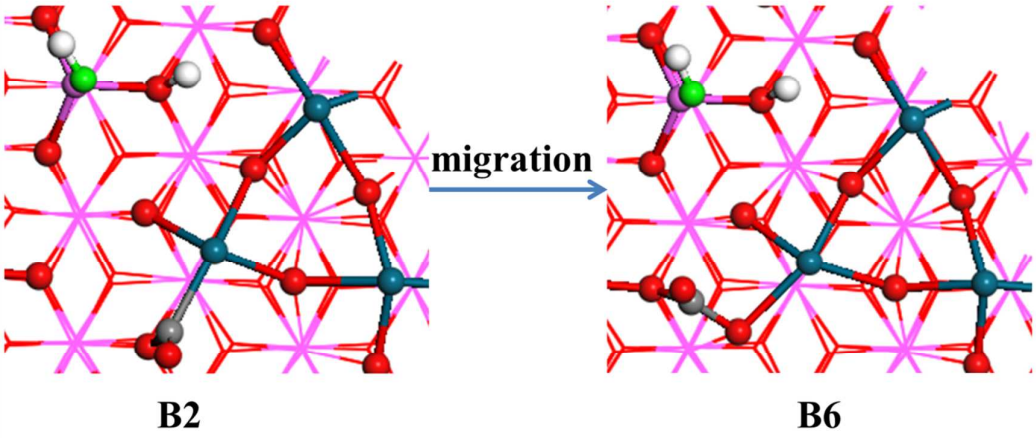

Fig. 8. The optimized stable structures of CO adsorption on the hy-Pd_3O_9@α-Al_2O_3(0001) surface. The grey ball denotes the C atom in CO.

A reaction mechanism is proposed as displayed in Fig. 9, in which the energetics are also shown. In this putative mechanism, the catalytic cycle is initiated by the adsorption of CO onto Pd (step i). After overcoming an activation barrier of 0.59 eV, an intermediate (step ii: carbonate-like, CO_3) is found, and there is a reaction with a surface oxygen atom coordinated with Pd (O_{Pd}). At the transition state (TS1), the C-O bond length and two C-O_{Pd} bond lengths are computed to be 1.187, 1.216 and 2.197 Å, respectively. After passing over TS1, a CO_2 molecule is generated completely and desorbed from the surface with an activation barrier of 0.76 eV and endothermic heat of 0.64 eV, resulting in an oxygen vacancy (O_v) near the Pd atoms (step iii). The oxidation reaction of the first CO_2 formation occurs through a Mars-van Krevelen mechanism[59]. Our results note that the formation of CO_3 is easier than the desorption of CO_2, which is the same as with the oxidation of CO along the path M_{ER2} reported by Sun[60] *et al*. The primary reason is that the carbonate-like intermediated CO_3 is very stable on the α-Al_2O_3(0001) surface.

Compared to the Mars-van Krevelen mechanism on the first half of the catalytic

cycle, the adsorption of O_2 competing with CO on the top of the Pd atom has been calculated (see Table. 4). On the top of the Pd atom, the adsorption energy of the O_2 molecule is -1.35 eV, which is lower than that of the CO molecule (-0.90 and 0.91 eV); this is less stable than the most favourable adsorption site (B2 site) of the CO molecule. The co-interaction of adsorbed CO and adsorbed O_2 molecules on the top of the Pd atom directly gives rise to intermediate OCOO, intermediate CO_3 or CO_2 gas and adsorbed O, respectively, which have high activation barriers of 1.91, 1.81 and 4.52 eV, respectively. It is clear that these significantly high barriers make the three paths less possible for CO oxidation. Thus, we believe that the oxidation reaction of the first CO_2 formation occurs through a Mars-van Krevelen mechanism.

Table 4. Activation barrier and reaction energy for CO oxidation along coadsorbed CO and O_2 on the top of the Pd atom. All energies are given in eV.

Reactant	Intermediate	Activation barrier (eV)	Reaction energy (eV)
$CO + O_2$	OCOO	1.91	1.94
	CO_3	2.81	-1.56
	CO_2+O	4.52	-0.56

According to the crude electron-pair Lewis theory of the chemical bond[61], removing an oxygen atom from the surface leaves behind two unpaired electrons. This means that an oxygen vacancy (O_v) is a strong Lewis base, which adsorbs O_2 strongly because O_2 is a strong Lewis acid.

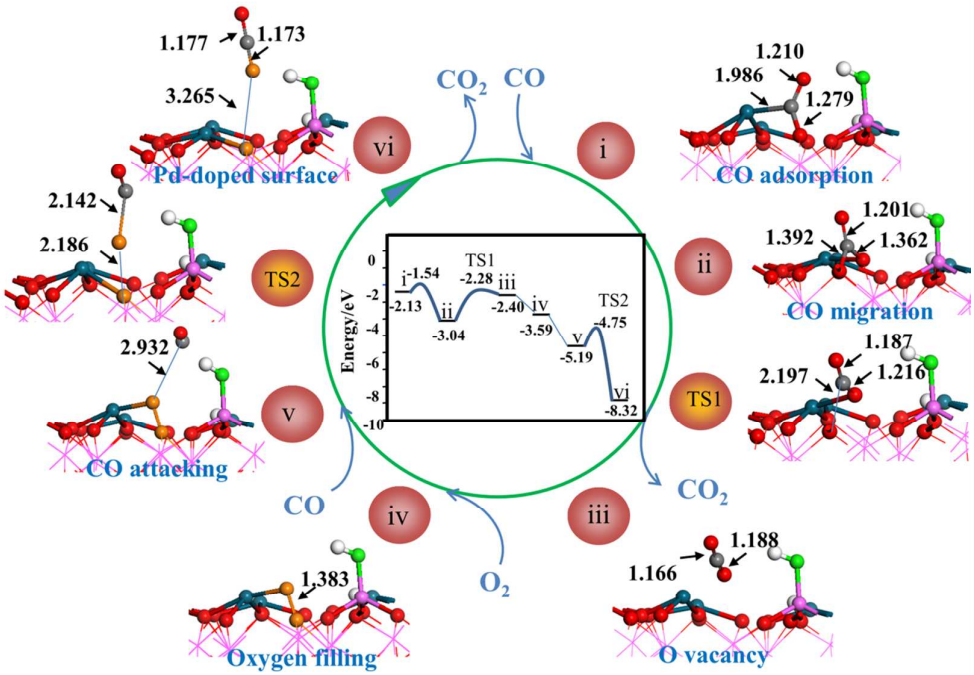

Fig. 9. Proposed reaction pathway for CO oxidation on the hydroxylated Pd_3O_9@α-Al_2O_3(0001) surface (side view). The orange balls denote O atoms in O_2. The energy and bond lengths are given in eV and angstroms, respectively.

The second half of the catalytic cycle starts with the newly formed oxygen vacancy from the first step, in which Pd is now coordinated to three surface oxygen atoms with distances of 1.968, 2.029 and 2.069 Å. Here, we first consider an Eley-Rideal (E-R) mechanism. The adsorption of an O_2 molecule at the vacancy is highly exothermic (E_{ads}=-1.35 eV), with its bond length elongated from 1.230 Å (O-O bond length of the isolated molecule) to 1.383 Å, which is the same as the CO adsorption on the Pd/γ-Al_2O_3(0001) surface[20]. Then, the CO gas promptly reacts with the pre-adsorbed O_2 on the O_v site. For step v, the distance between the carbon atom in CO and the oxygen atom in adsorbed O_2 is 2.932 Å, indicating the weak interaction between the CO molecule and the adsorption of the pre-adsorbed O_2. In the transition state (TS2), the distance between the carbon atom in CO and the oxygen atom in

adsorbed O_2 decreases to 2.142 Å, and the bond length of the O-O in O_2 increases from 1.383 to 2.186 Å, suggesting the formation of the CO_2 molecule. Through TS2, a CO_2 molecule is generated completely and desorbed from the surface. This step has an energy barrier of 0.44 eV, and the exothermicity is found to be 3.13 eV. By releasing the CO_2 product, the Pd recovers its tetra-coordinated state on the hydroxylated Pd_3O_9@α-Al_2O_3(0001) surface.

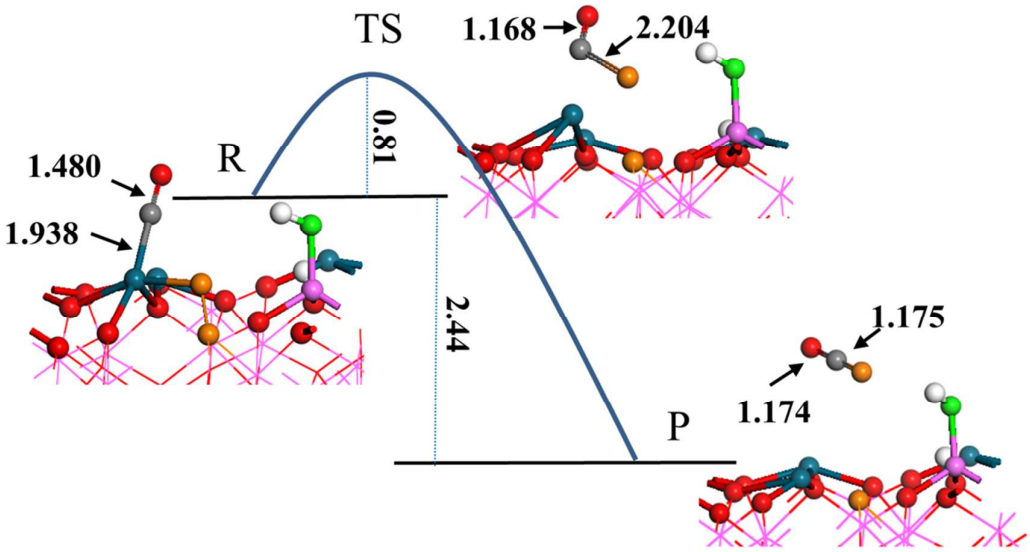

Fig. 10. Proposed reaction pathway for CO oxidation on the hy-Pd_3O_9@α-Al_2O_3(0001) surface via L-H mechanism. The bond lengths and energies are given in angstroms and eV, respectively.

Compared to the E-R mechanism on the second half of the catalytic cycle, the Langmuir-Hinshelwood (L-H) mechanism has been calculated (see Fig. 10). The CO and the pre-adsorbed O_2 on the O_v site are co-adsorbed on the hy-Pd_3O_9@α-Al_2O_3(0001) surface. The binding energy of the CO adsorption on the Pd atom is -1.27 eV (R). One oxygen atom in the pre-adsorbed O_2 molecule starts to approach the carbon atom in the adsorbed CO to reach the transition state (TS), resulting in the distance between the carbon atom in the adsorbed CO and the oxygen

atom in the pre-adsorbed O_2 molecule decreasing from 2.869 to 2.204 Å. The calculated activation barrier for the reaction is 0.81 eV. Passing after the release of the second CO_2 molecule from the surface, the remaining O atom in the pre-adsorbed O_2 molecule restores the hy-Pd_3O_9@α-Al_2O_3(0001) surface. Compared to the calculated activation energy barrier (0.44 eV) in the E-R mechanism, the barrier (0.81 eV) is much higher in the case of the L-H mechanism. Therefore, the formation of the second CO_2 molecule is most likely through the E-R mechanism.

3.4 CO oxidation cycle on ideal α-Al_2O_3(0001) surface

In this putative mechanism (Fig. 11, blue line, M_{ER1}), the catalytic cycle is initiated by the adsorption of CO onto Al (R). After overcoming an activation barrier of 1.72 eV, a CO_2 molecule is generated completely, which results in an oxygen atom being adsorbed on top of the Al atom. In the transition state (TS3), the distance between the carbon atom in CO and the oxygen atom in O_2 decreases from 2.634 to 1.424 Å, and the bond length of the O-O in O_2 increases from 1.250 to 1.381 Å. The significantly high barrier makes the M_{ER1} path less possible for CO oxidation on α-Al_2O_3(0001) surface.

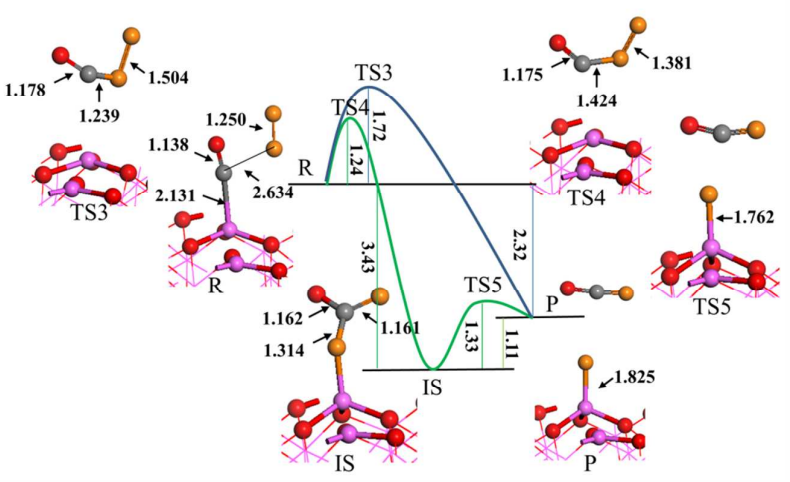

Fig. 11. Proposed reaction pathway for CO oxidation on the α-Al_2O_3(0001) surface via E-R mechanism. The bond lengths and energies are given in angstroms and eV, respectively.

After testing different possible co-adsorption configurations, we found the stable configuration, which is the carbonate-like (CO_3) compound. Another path (Fig. 11, green line, M_{ER2}) is considered in which adsorbed CO reacts with the O_2 molecule to form an intermediate (IS: carbonate-like, CO_3), via TS4, with an activation barrier of 1.24 eV and exothermic heat of 3.43 eV. In the next desorption path from CO_3 to the final product of CO_2 gas, an energy barrier of 1.33 eV (TS5) is needed. The barriers involved in this path are not too large to be surmounted; however, compared to the calculated activation energy barrier of CO oxidation on the hy-Pd_3O_9@α-Al_2O_3(0001) surface, the barrier of that on α-Al_2O_3(0001) surface is much higher, and the results indicate that the energy barrier for CO oxidization is obviously reduced compared to the undoped case, which implies that the introduction of Pd can efficiently improve the oxidation reactivity of the α-Al_2O_3(0001) surface.

According to the above results, it is clear that the mechanism of CO oxidation on the hy-Pd_3O_9@α-Al_2O_3(0001) surface occurs first by CO adsorption and migration,

second by O_v formation with the first CO_2 release, then by the first foreign O_2 filling and CO co-adsorption, and finally by the second CO_2 desorption and restoration of the hy-Pd_3O_9@α-Al_2O_3(0001) surface. Our calculated results reveal that the high activation barrier (0.76 eV) on the surface indicates the formation of TS1, the rate-determination step in the whole catalytic cycle, which is lower than that of CO oxidation at synthesized Ir_1/FeO_x (1.41 eV)[19] and equal to that of CO oxidation at synthesized Pt_1/FeO_x (0.79 eV)[2]. Therefore, the Pd_3O_9@α-Al_2O_3 catalyst shows superior catalytic activity for CO oxidation.

4. Conclusions

Because of the considerable importance of palladium-based and doped metal-oxide catalysts in CO oxidation, we designed a new Pd_3O_9@α-Al_2O_3 catalyst and simulated the hydroxylated effect. In this paper, the structure, electronic properties, and oxidation activity of hy-Pd_3O_9@α-Al_2O_3(0001) surface have been investigated by DFT. A total of ten configurations of doping models considering hydroxylation were calculated. Our results indicate that the Pd element preferentially replaces the Al atom under the O-rich growth condition. The lowest formation energy of Pd-doped clean and hydroxylated α-Al_2O_3(0001) surface is 0.21 eV under the conditions in which the coverage of Pd-doped α-Al_2O_3 is 0.75 on a pre-hydroxylated surface and the water coverage is 0.25, which leads to the formation of a Pd_3O_9 cluster embedded in the Al_2O_3(0001) surface. Furthermore, owing to the combination of an optimized structure and partial DOS and Mulliken charges, the O_{Pd} atoms in the Pd_3O_9 cluster are easier to remove and are also more reactive, which agrees with the previous report.

Theoretical calculations have been performed to explore the catalytic mechanism and activity of the new hy-Pd_3O_9@α-Al_2O_3 catalyst for CO oxidation. We proposed a catalytic mechanism of CO oxidation on the hy-Pd_3O_9@αAl_2O_3 catalyst. The reaction mechanisms have been elucidated first by CO adsorption and migration, second by O_v formation with the first CO_2 release, then by the first foreign O_2 filling and CO co-adsorption, and finally by the second CO_2 desorption and restoration of the hy-Pd_3O_9@α-Al_2O_3(0001) surface. The rate determination step is the formation of the first CO_2 in the whole catalytic cycle. Furthermore, compared to the undoped surface, the energy barrier for CO oxidization is obviously reduced from 1.33 eV for the pure surface to 0.76 eV for Pd-doped surface (D_{pd}=0.75), which implies that the introduction of Pd can efficiently improve the oxidation reactivity of the α-Al_2O_3(0001) surface. The calculation results also show that the formation of the first CO_2 molecule is the rate-determination step (activation barrier 0.76 eV) in the whole catalytic cycle, which is lower than that of CO oxidation at synthesized Ir_1/FeO_x (1.41 eV)[19] and Pt_1/FeO_x (0.79 eV)[2]. Therefore, the Pd_3O_9@α-Al_2O_3 catalyst shows superior catalytic activity for CO oxidation. The present results enrich the understanding of the catalytic oxidation of CO by palladium-based catalysts and provide a clue for fabricating palladium-based catalysts with low cost and high activity. It is hoped that our theoretical study will provide experiments with instructive information on further exploring the intriguing chemistry of CO oxidation on palladium-based catalysts and may be beneficial to the further replacement of high-priced noble metal catalysts.

Acknowledgements

This work is supported by NSFC projects (Nos. 21201165, and 21171165) and FJPNSF project (2013J05040). We acknowledge the Supercomputing Centre of CNIC for providing the computer resources.

References

1. A. Comas-Vives, C. Gonzalez-Arellano, A. Corma, M. Iglesias, F. Sánchez and G. Ujaque, *J. Am. Chem. Soc.*, 2006, **128**, 4756-4765.
2. B. Qiao, A. Wang, X. Yang, L. F. Allard, Z. Jiang, Y. Cui, J. Liu, J. Li and T. Zhang, *Nat. Chem.*, 2011, **3**, 634-641.
3. Y. Huang, A. Wang, L. Li, X. Wang, D. Su and T. Zhang, *J. Catal.*, 2008, **255**, 144-152.
4. XIAO-FENG YANG, AIQIN WANG, BOTAO QIAO, JUN LI, JINGYUE LIU and T. ZHANG, *Acc. Chem. Res.*, 2013, **46**, 1740-1748.
5. S. Y. Peng, Z. N. Xu, Q. S. Chen, Y. M. Chen, J. Sun, Z. Q. Wang, M. S. Wang and G. C. Guo, *Chem. Commun.*, 2013, **49**, 5718-5720.
6. A. Y. Yin, X. Y. Guo, W. L. Dai and K. N. Fan, *Chem. Commun.*, 2010, **46**, 4348-4350.
7. Qiaohong Li, Zhangfeng Zhou, Ruiping Chen, Baozhen Sun, Luyang Qiao, Yuangen Yao and K. Wu, *Phys. Chem. Chem. Phys.*, 2015, **17**, 9126-9134.
8. Y. Zhang and A. Bell, *J. Catal.*, 2008, **255**, 153-161.
9. L. Zhang, A. Wang, J. T. Miller, X. Liu, X. Yang, W. Wang, L. Li, Y. Huang, C.-Y. Mou and T. Zhang, *ACS Catal.*, 2014, **4**, 1546-1553.
10. R. Q. Zhang, T. H. Lee, B. D. Yu, C. Stampfl and A. Soon, *Phys. Chem. Chem. Phys.*, 2012, **14**, 16552-16557.
11. Y. Tang, Z. Yang and X. Dai, *Phys. chem. chem. phys.*, 2012, **14**, 16566-16572.
12. S. Li, X. Lu, W. Guo, H. Zhu, M. Li, L. Zhao, Y. Li and H. Shan, *J. Organ. Chem.*, 2012, **704**, 38-48.
13. K. Mao, L. Li, W. Zhang, Y. Pei, X. C. Zeng, X. Wu and J. Yang, *Sci. Rep.*, 2014, **4**, 5441.
14. T. K. Ghosh and N. N. Nair, *ChemCatChem*, 2013, **5**, 1811-1821.
15. M. Moses-DeBusk, M. Yoon, L. F. Allard, D. R. Mullins, Z. Wu, X. Yang, G. Veith, G. M. Stocks and C. K. Narula, *J. Am. Chem. Soc.*, 2013, **135**, 12634-12645.
16. J. Lin, A. Wang, B. Qiao, X. Liu, X. Yang, X. Wang, J. Liang, J. Li, J. Liu and T. Zhang, *J. Am. Chem. Soc.*, 2013, **135**, 15314-15317.
17. W.-C. Ding, X.-K. Gu, H.-Y. Su and W.-X. Li, *J. Phys. Chem. C*, 2014, **118**, 12216-12223.
18. Z. Huang, X. Gu, Q. Cao, P. Hu, J. Hao, J. Li and X. Tang, *Angew. Chem. Int. Ed.*, 2012, **51**, 4198-4203.
19. J.-X. Liang, J. Lin, X.-F. Yang, A.-Q. Wang, B.-T. Qiao, J. Liu, T. Zhang and J. Li, *J. Phys. Chem. C*, 2014, **118**, 21945-21951.
20. E. J. Peterson, A. T. DeLaRiva, S. Lin, R. S. Johnson, H. Guo, J. T. Miller, J. Hun Kwak, C. H. Peden, B. Kiefer, L. F. Allard, F. H. Ribeiro and A. K. Datye, *Nat. Commun.*, 2014, **5**, 4885-4895.

21. S. Lin, X. Ye, R. S. Johnson and H. Guo, *J. Phys. Chem. C*, 2013, **117**, 17319-17326.
22. X. Liu, T. Duan, C. Meng and Y. Han, *RSC Adv.*, 2015, **5**, 10452-10459.
23. A. D. Zdetsis and A. B. Kunz, *Phys. Rev. B*, 1985, **32**, 6358.
24. M. Valero, P. Raybaud and P. Sautet, *J. Catal.*, 2007, **247**, 339-355.
25. M. Valero, P. Raybaud and P. Sautet, *Phys. Rev. B*, 2007, **75**, 045427.
26. J. Gomes, F. Illas, N. C. Hernández, A. Márquez and J. Sanz, *Phys. Rev. B*, 2002, **65**, 125414.
27. V. V.Rivanenkov, V. A.Nasluzov, A. M.Shor, K. M.Neyman and N. R. o. osch, *Surf. Sci.*, 2003, **525**, 173-183.
28. M. Corral Valero, P. Raybaud and P. Sautet, *J. Phys. Chem. B*, 2006, **110**, 1759-1767.
29. B. E. Nieuwenhuys, *Adv. Catal.*, 1999, **44**, 259-328.
30. J. Gustafson, R. Westerström, A. Mikkelsen, X. Torrelles, O. Balmes, N. Bovet, J. N. Andersen, C. Baddeley and E. Lundgren, *Phy. Rev. B*, 2008, **78**, 045423.
31. Y.-G. Wang, Y. Yoon, V.-A. Glezakou, J. Li and R. Rousseau, *J. Am. Chem. Soc.*, 2013, **135**, 10673-10683.
32. M. Okumura, N. Masuyama, E. Konishi, S. Ichikawa and T. Akita, *J. Catal.*, 2002, **208**, 485-489.
33. S. D. Gardner, G. B. Hoflund, B. T. Upchurch, D. R. Schryer, E. J. Kielin and J. Schryer, *J. Catal.*, 1991, **129**, 114-120.
34. Y. Li, Y. Yu, J.-G. Wang, J. Song, Q. Li, M. Dong and C.-J. Liu, *Appl. Catal. B: Environ.*, 2012, **125**, 189-196.
35. K. Ruth, M. Hayes, R. Burch, S. Tsubota and M. Haruta, *Appl. Catal. B,*, 2000, **24**, 133-138.
36. X. Liu, Y. Sui, T. Duan, C. Meng and Y. Han, *Phys. Chem. Chem. Phys.*, 2014, **16**, 23584-23593.
37. X. Tang, J. Schneider, A. Dollinger, Y. Luo, A. Wörz, K. Judai, S. Abbet, Y. Kim, G. Ganteför and D. Fairbrother, *Phys. Chem. Chem. Phys.*, 2014, **16**, 6735-6742.
38. S.-Y. Wang, N. Li, L.-F. Luo, W.-X. Huang, Z.-Y. Pu, Y.-J. Wang, G.-S. Hu, M.-F. Luo and J.-Q. Lu, *Appl. Catal. B: Environ.*, 2014, **144**, 325-332.
39. C. Tang, J. Sun, X. Yao, Y. Cao, L. Liu, C. Ge, F. Gao and L. Dong, *Appl. Catal. B: Environ.*, 2014, **146**, 201-212.
40. Y. Yamamoto, *Catal. Surv. Asia*, 2010, **14**, 103-110.
41. Z.-N. Xu, J. Sun, C.-S. Lin, X.-M. Jiang, Q.-S. Chen, S.-Y. Peng, M.-S. Wang and G.-C. Guo, *ACS Catal.*, 2013, **3**, 118-122.
42. Ludovic G. V. Briquet, C. Richard A. Catlow and S. A. French, *J. Phys. Chem. C*, 2008, **112**, 18948-18954.
43. C. Rohmann, J. B. Metson and H. Idriss, *Phys. Chem. Chem. Phys.*, 2014, **16**, 14287-14297.
44. B. Delley, *J. Chem. Phys.*, 1990, **92**, 508-517.
45. B. Delley, *J. Chem. Phys.*, 2000, **113**, 7756-7764.
46. J. P. Perdew and Y. Wang, *Phys. Rev. B*, 1992, **45**, 13244-13249.
47. L. Versluis and T. Ziegler, *J. Chem. Phys.*, 1988, **88**, 322-328.
48. U. von Barth and L. Hedin, *J. Phys. C: Solid State Phys.*, 1972, **5**, 1629-1642.
49. C.-S. Lee, T.-S. Hwang, Y. Wang, S.-M. Peng and C.-S. Hwang, *J. Phys. Chem.*, 1996, **100**, 2934-2941.
50. Z. G. Wang, Q. D. Zeng, Y. B. Luan, X. J. Wu, L. J. Wan, C. Wang, G. U. Lee, S. X. Yin, J. L. Yang and C. L. Bai, *J. Phys. Chem. B*, 2003, **107**, 13384-13388.
51. T. T. Lin, W.-D. Zhang, J. C. Huang and C. B. He, *J. Phys. Chem. B*, 2005, **109**, 13755-13760.
52. N. Matsuzawa, J. e. Seto and D. A. Dixon, *J. Phys. Chem. A*, 1997, **101**, 9391-9398.

53. C. Persson, Y.-J. Zhao, S. Lany and A. Zunger, *Phys. Rev. B*, 2005, **72**, 035211.
54. C. Arhammar, M. Araujo and R. Ahuja, *Phys. Rev. B.*, 2009, **80**, 115208.
55. R. Long and N. J. English, *J. Phys. Chem. C*, 2009, **113**, 9423-9430.
56. H. Jin, J. Zhu, W. Chen, Z. Fang, Y. Li, Y. Zhang, X. Huang, K. Ding, L. Ning and W. Chen, *J. Phys. Chem. C*, 2012, **116**, 5067-5075.
57. Y. Zhang, L. Giordano and G. Pacchioni, *J. Phys. Chem. C*, 2007, **111**, 7437-7445.
58. X. Liu, Y. H. Sui, T. Duan, C. G. Meng and Y. Han, *Catal. Sci. Technol.*, 2015, **5**, 1658-1667.
59. P. Mars and D. W. van Krevelen, *Chem. Eng. Sci. Spec. Suppl.*, 1954, **3**, 41-59.
60. B. Z. Sun, W. K. Chen and Y. J. Xu, *J. Chem. Phys.*, 2010, **133**, 154502.
61. G. N. Lewis, *J. Chem. Phys*, 1933, **1**, 17.

Figure captions

Fig. 1. Top view of the optimised stable geometry of α-Al_2O_3(0001) surface.

Fig. 2. The formation energy (ΔE_{form}, eV) of adsorbed H_2O onto Pd@α-Al_2O_3(0001) surface.

Fig. 3. Top view of the optimised stable geometry. Hy is defined as hydroxylated.

Fig. 4. Partial DOS of Pd_3O_9@α-Al_2O_3(0001) surface. The Fermi level is set at zero. O_{3f_pd} defines the three-coordination surface O atom, which is close to Pd atom; and O_{4f} defines the four-coordination surface O atom, which is close to Pd atom.

Fig. 5. The value of Mulliken charges of clean α-Al_2O_3(0001) surface (A), Pd_3O_9@α-Al_2O_3(0001) surface (B) and hydroxylated Pd_3O_9@α-Al_2O_3(0001) (C). The pink, dark blue, and red sticks denote Al, Pd and O atoms, respectively.

Fig. 6. Top and side views of the optimised stable geometry for Hy- Pd_3O_9@α-Al_2O_3(0001) surface. The dark blue, pink, red, green and white balls denote Pd, Al, O, O in OH and H atoms, respectively. The same colour scheme is applied in **Figs. 8–11**.

Fig. 7. Top view of the optimised stable geometry of single CO adsorption on hydroxylated Pd_3O_9@α-Al_2O_3(0001).

Fig. 8. The optimized stable structures of CO adsorption on the hydroxylated Pd_3O_9@α-Al_2O_3(0001) surface. The grey ball denotes the C atom in CO.

Fig. 9. Proposed reaction pathway for CO oxidation on the hydroxylated Pd_3O_9@α-Al_2O_3(0001) surface (side view). The orange balls denote the O atoms in O_2. The energy and bond lengths are given in eV and angstroms, respectively.

Fig. 10. Proposed reaction pathway for CO oxidation on the hydroxylated Pd_3O_9@α-Al_2O_3(0001) surface via L-H mechanism. The bond lengths and energies are given in Å and eV, respectively.

Fig. 11. Proposed reaction pathway for CO oxidation on the α-Al_2O_3(0001)surface via E-R mechanism. The bond lengths and energies are given in angstroms and eV, respectively.